Article Submitted to Bulletin of Mathematical Biology

Growth and function of fungal mycelia in heterogeneous environments

Graeme P. Boswell[1], Helen Jacobs[2], Fordyce A. Davidson*[1], Geoffrey M. Gadd[2] and Karl Ritz[3]

[1]*Department of Mathematics, University of Dundee, Dundee, DD1 4HN, U.K.*

[2]*Division of Environmental and Applied Biology, Biological Sciences Institute, School of Life Sciences, University of Dundee, Dundee, DD1 4HN, U.K.*

[3]*Soil-Plant Dynamics Group, Scottish Crop Research Institute, Invergowrie, DD2 5DA, U.K. (Current permanent address: National Soil Resources Institute, Cranfield University, Silsoe, MK45 4DT, U.K.)*

Abstract

As decomposer organisms, pathogens, plant symbionts and nutrient cyclers, fungi are of fundamental importance in the terrestrial environment. Moreover, in addition to their well-known applications in industry, many species also have great potential in environmental biotechnology. The study of this important class of organisms is difficult through experimental means alone due to the heterogeneity of their natural growth habitat and the microscopic scale of growth. In this work we present a mathematical model for colony expansion that is derived through consideration of the growth characteristics on the microscale. The model equations are of mixed hyperbolic-parabolic type and are treated with a numerical scheme that preserves positivity and conserves mass. The resulting numerical solutions are compared against experimental results in a variety of environments. Thus the effect of different translocation mechanisms on fungal growth and function are identified. The derivation and analysis of an approximation to the full model, yields further results concerning basic properties of mycelial growth. Finally, the acidification of the growth habitat is considered and the model thus provides important predictions on the functional consequences of the redistribution of internally-located material.

1. Introduction

In the terrestrial environment, fungi are of fundamental importance as decomposer organisms, pathogens and plant symbionts (mycorrhizas), playing im-

*Author for correspondence: fdavidso@maths.dundee.ac.uk

portant roles in carbon, nitrogen, phosphorus and other biogeochemical cycles (Wainwright, 1988; Gadd, 1999). The formation of mycorrhizas with the majority of plant species allows transfer and redistribution of nutrients over far wider spatial scales than would be possible in their absence (Boddy, 1999). Free-living fungi are often dominant in acidic conditions (Morley et al., 1996), and in soil can comprise the largest pool of biomass (including other microorganisms and invertebrates) (Metting, 1992). This, combined with their branching, explorative growth habit and high surface area to mass ratio ensures that fungi are an integral component of major environmental cycling processes. Furthermore, apart from their established importance in industry, e.g. alcohol, antibiotic and citric acid manufacture, many species have great potential in areas of environmental biotechnology including biological control (Jin et al., 1992; Trujillo, 1992) and bioremediation of soil and water contaminated with organic and inorganic pollutants (Gadd, 1992, 1993, 2001; Gadd and White, 1993; Burgstaller and Schinner, 1993; Alexander, 1994; Tobin et al., 1994; Gadd and Sayer, 2000).

The spatio-temporal distribution of nutrients and minerals is heterogeneous in most natural environments. In soils, where the complex particulate structure further enhances environmental heterogeneity, this is especially true. Filamentous fungi (i.e. species that form a mycelium consisting of an indeterminate system of apically-extending branching tubes termed *hyphae*) are well adapted to growth in such environments as their thread-like hyphae can grow across surfaces, through pores and across air gaps. Translocation – the redistribution of internally-located material through the hyphal network – further enhances the ability of certain fungi to grow in such patchy environments. Indeed, it is now known that many fungi are able to grow in low-nutrient or other inhospitable environments by exploiting the resources available to other parts of the mycelium and using translocation to supplement colony growth (see, for example, Olsson, 1995; Ritz, 1995; Boddy, 1999). In this paper we consider the growth dynamics of mycelial fungi in general, and *Rhizoctonia solani* in particular, and construct a model that relates the microscopic behaviour of individual hyphae to colony growth and function.

The detailed review by Prosser (1995) summarizes much of the mathematical modelling of fungal growth up to that date. In general, modelling has either focussed on the macroscopic level, using quantities such as biomass yield (e.g. Paustian and Schnürer, 1987), or has focussed on growth on the microscopic level by considering events such as hyphal tip growth, branching and anastomosis – the fusion of hyphal tips into hyphal walls (e.g. Heath, 1990). In the former, spatial properties are in general ignored while in the latter, temporal effects are neglected.

In a series of papers, Edelstein (1982), Edelstein and Segel (1983), Edelstein-Keshet and Ermentrout (1989) (hereafter collectively referred to as Edelstein-Keshet et al.) link the microscopic behaviour of individual hyphae to the macroscopic behaviour of the fungal colony as a whole. Their models are systems of partial differential equations (PDEs) where the variables denote hyphal density,

hyphal tip density and the concentration of a growth-limiting substrate. The substrate exists in two forms, either located within the mycelium or free in the external environment: the distinction between internal and external substrate allows translocation to be explicitly modelled (the variables depend on both space and time).

Davidson et al. (1996), Davidson (1998), Davidson and Olsson (2000) and references therein (hereafter collectively referred to as Davidson et al.) provide an alternative description of fungal growth by focusing on the macroscopic development of fungal mycelia. In Davidson (1998) the system comprises three main elements: a biomass density, an internal substrate concentration and an external substrate concentration, and translocation is assumed to occur purely by diffusion inside the biomass network. Fungal growth and subsequent substrate depletion is modelled by a system of reaction-diffusion equations, where the flux and reaction terms are chosen to represent important qualitative features associated with mycelial growth. An active translocation mechanism was introduced in Davidson and Olsson (2000) where the flux of internally-located material is modelled via a convection term (where the velocity is substrate dependent) and is directed towards the edge of the fungal colony. The results are in good qualitative and quantitative agreement with experiments on out-growth of *Arthrobotrys superba* in nutrient-free environments (Persson et al., 2000).

More recently, Boswell et al. (2002) derived a fungal growth model by combining elements from the work of Edelstein-Keshet et al. and Davidson et al. and by reformulating the manner in which certain processes are modelled. In particular, the mechanisms responsible for substrate translocation are reconsidered giving rise to a model having bi-directional active *and* passive translocation. The solution of this model is highly non-trivial and thus a suitable numerical method was developed and is described in Boswell et al. (2003). The model parameters were carefully calibrated for the fungus *Rhizoctonia solani* via a specific set of growth experiments resulting in very good qualitative and quantitative agreement between model and simple experimental systems.

In this work we consider a more general growth model which again focuses on the properties of *Rhizoctonia solani*. In particular, unlike previous studies, our model includes a mechanism that generates the directed (but non-chemotactic) growth typically exhibited by fungal hyphae and thus allows the modelling of mycelial growth in all spatial dimensions.(In previous studies, mycelial growth was modelled either as a purely diffusive process or as a purely convective process directed away from the site of inoculation.) Therefore, this model allows for a much more detailed comparison with complex experimental assays comprising heterogeneous distributions of nutrients and minerals (see Jacobs et al., 2002).

In Section 2, a model of fungal growth is derived by considering growth characteristics at the microscopic level. The resulting model equations are of mixed hyperbolic-parabolic type and require great care in their solution to obtain meaningful and accurate results. Therefore, in Section 3 (and more fully in Appendix A), we describe the numerical method developed to obtain solutions of the model

equations. The model is calibrated using data provided by growth experiments for the fungus *R. solani* at 30°C in a standard medium. Various growth habitats are considered in Sections 4 & 5 and we compare model solutions with experimental observations. In addition, the acidification of the growth habitat is modelled since this property is important for the solubility of toxic metals and their compounds, and in agricultural applications (solubilisation of metal phosphates). Finally, in Section 6, the implications of the modelling results are discussed and we comment on the biotechnological uses of fungi.

2. Physiology and Modelling

Fungi are well adapted for growth in soils due to their branching networks and explorative filamentous growth habit. With few exceptions, hyphae elongate strictly by apical deposition of wall skeletal polysaccharides, especially chitin and β-glucans (Gooday, 1995). Inherent in apical growth is the forward transport of a range of types of vesicles, which provide new cell membrane material. The vesicles carrying materials such as membrane-bound enzymes and extracellular enzymes, accumulate in the apical body also known as the Spitzenkörper. Steady movement forward of the vesicles gives rise to an extending hypha (Gooday, 1995). The extension of the hyphal tip enables the hyphae to penetrate solid substrata such as chitin, and excretion of lytic enzymes by the growing tips digests external polymers, converting them into products small enough to be taken up as nutrients by the fungus (Wessels, 1993; Sietsma et al., 1995). The transport of nutrients in the form of solutes into and out of the cytoplasm across the plasma membrane and assorted endomembranes of fungal cells is essential for their survival (Garrill, 1995).

Rhizoctonia solani J. G. Kühn is an economically important species of fungus as it can infect a wide range of host plants and occurs throughout the world in both cultivated and non-cultivated soils (Ogoshi, 1987). Strains of *R. solani* are categorized on the basis of pathogenicity on specific host plants and by anastomosis groups. Fusion of two mycelial isolates via the tip cells indicates an anastomosis group and allows gene transfer between different strains (McCabe et al., 1999). Although *R. solani* is an asexual fungus, it can persist in soils for long periods of time by the production of sclerotia, which are hardened masses of hyphae (Alexopolous et al., 1996).

R. solani is predominately known as a plant pathogenic fungus. However non-pathogenic binucleate strains of *R. solani* are currently being developed for biological control purposes (Cartwright and Spurr, 1998). The strong saprophytic capabilities of *R. solani* have also been recognised (Thornton and Gilligan, 1999; Bailey et al., 2000) as transmission of disease by pathogenic fungi is dependent on their ability to grow through soils in the absence of a host (Otten et al., 1999).

Translocation is an important process that allows the redistribution of metabolites within the fungal mycelium. The ability of *R. solani* to translocate has long been acknowledged (Littlefield et al., 1964) while more recent studies have fo-

cussed on the role of translocation for the growth of *R. solani* in heterogeneous environments (Olsson, 1994; Ritz, 1995; Jacobs et al., 2002). In particular, Olsson (1995) showed that at least two translocation mechanisms were responsible for nutrient reallocation in *R. solani*: simple diffusion, and the active movement of intracellular metabolites from regions of local excess to regions of local scarcity.

We will model the interaction of the fungal mycelium with its (heterogeneous) environment in the following way. The mycelium will be considered as a continuous distribution consisting of three components: active hyphal density, inactive hyphal density and hyphal tip density. *Active hyphae* refer to those hyphae involved in the translocation of internal metabolites while *hyphal tips* denote the ends of these hyphae. *Inactive hyphae* denote hyphae no longer directly involved in translocation, branching or anastomosis representing, for example, vacuolated hyphae.

We distinguish between nutrients located within the fungus (internal) and those free in the outside environment (external). Internally-located material is used to extend hyphal tips and effectively is converted into the biomass "trail" left behind a tip as it moves. In most environments, a suitable combination of nutrients is required for growth: of particular importance are carbon and nitrogen as well as phosphorus, sulphur and trace elements. In this paper, we assume that a single, generic substance is limiting for growth. We consider this substance to be carbon not only because of its central role in fungal heterotrophy, but also because (i) nitrogen was abundant (not "limiting") in the experimental system used to calibrate the model (Boswell et al., 2002), and (ii) *R. solani* possesses both active and passive translocation mechanisms for carbon (Olsson, 1995).

The model thus consists of five variables: active hyphal density $m(\boldsymbol{x}, t)$; inactive hyphal density $m'(\boldsymbol{x}, t)$; hyphal tip density $p(\boldsymbol{x}, t)$; internal substrate concentration $s_i(\boldsymbol{x}, t)$; and external substrate concentration $s_e(\boldsymbol{x}, t)$.

The growth dynamics of *R. solani* (and indeed all fungi) are greatly influenced by the presence of physical boundaries. In this paper we will not consider the effects of such boundaries and instead focus on nutritional heterogeneity. The growth experiments discussed in this paper were conducted in a circular 9 cm diameter Petri dish by inoculating the test fungus at the centre of the dish. All observations were made before the fungus reached the edge of the dish. In this system, the external nutritional environment (the tessellations of agar droplets, see below) can be modelled as being essentially two-dimensional. (We are assuming that the depth of the agar is sufficiently small as to allow the gradient in substrate concentration in that direction to be neglected.) One can also view the mycelium as being essentially two-dimensional. As has been observed, the structure of a mycelium is generally fractal, typically having a dimension between 1.4 and 2.0 (Ritz and Crawford, 1990). Hence, once nutrients are absorbed into the mycelium, they must move within this fractal network. Transit times of substrate molecules are consequently reduced i.e., the time taken for a substrate molecule to diffuse a given distance within the network is less than the corresponding time in the external environment (see, for example, Segel, 1980). However, to fully

include the fractal structure into the model would vastly increase its complexity and render it almost unusable in application. Hence, as a reasonable alternative, we view the mycelium as a two-dimensional structure but with an *effective* diffusion coefficient that captures the expected decrease in transit times (the substrate diffusion coefficient will be larger for internal substrate than external substrate). Note that approximate planar mycelial growth in 'natural' environments is quite common, e.g. on plant, animal and other surfaces.

The interactions between the components of the model are given by the following equations, which are obtained through standard mass conservation laws:

$$\frac{\partial m}{\partial t} = \underbrace{f_m(m, m', p, s_i, s_e)}_{\text{new hyphae}-\text{inactivated hyphae}}, \tag{1a}$$

$$\frac{\partial m'}{\partial t} = \underbrace{f_{m'}(m, m', p, s_i, s_e)}_{\text{inactivated hyphae}-\text{degradation}}, \tag{1b}$$

$$\frac{\partial p}{\partial t} = \underbrace{-\nabla \cdot \boldsymbol{J}_p(m, m', p, s_i, s_e)}_{\text{tip migration}} + \underbrace{f_p(m, m', p, s_i, s_e)}_{\text{branching}-\text{anastomosis}}, \tag{1c}$$

$$\frac{\partial s_i}{\partial t} = \underbrace{-\nabla \cdot \left(\boldsymbol{J}_i^{pas}(m, m', p, s_i, s_e) + \boldsymbol{J}_i^{act}(m, m', p, s_i, s_e)\right)}_{\text{passive \& active translocation}} + \underbrace{f_i(m, m', p, s_i, s_e)}_{\text{uptake}-\text{growth costs}-\text{trans. costs}}, \tag{1d}$$

$$\frac{\partial s_e}{\partial t} = \underbrace{-\nabla \cdot \boldsymbol{J}_e(m, m', p, s_i, s_e)}_{\text{diffusion}} + \underbrace{f_e(m, m', p, s_i, s_e)}_{-\text{uptake}}, \tag{1e}$$

where $\boldsymbol{J}$ and f respectively denote the flux and reaction terms for each variable. We now describe the form of the reaction and the flux terms, commencing with f_m. In all that follows $|\cdot|$ will denote the standard Euclidean norm in $\mathbb{R}^2$.

Tip extension is the primary means of fungal growth. A single hypha may therefore be regarded as the "trail" left behind a hyphal tip as it moves. Consequently the amount of hyphae created in a region over a given interval of time is simply the number of tips in that region multiplied by the averaged distance moved, i.e. $|\boldsymbol{J}_p|$, the absolute value of the tip flux. It is common that parts of the mycelium cease to be involved in translocation (for example, through vacuolation) as new hyphae are created. In certain species of fungi this inactivation seems to be an age-related property. However, no direct experimental evidence exists for such inactivation in *R. solani*. Moreover, we have observed that dormant (i.e. inactive) hyphae can be "revitalized" producing new branching and growth by additions of fresh nutrients (Jacobs et al., unpublished observations). In the absence of detailed experimental evidence, we model the inactivation by

a Poisson process of constant rate d_a. Thus we model f_m as

$$f_m = |\boldsymbol{J}_p| - d_a m. \tag{2}$$

In certain circumstances, inactive hyphae can autolyse and/or degrade in the environment to provide nutrients for plants, other micro-organisms or for the fungus itself. Again in the absence of further experimental evidence, we model this transition by a Poisson process of constant rate d_i. Consistent with the formulation of (2), we therefore set

$$f_{m'} = d_a m - d_i m'. \tag{3}$$

Now consider the reaction term f_p, corresponding to the creation and loss of hyphal tips. In filamentous fungi there are three distinct types of branching process: (i) dichotomous branching – the splitting of one tip to produce two tips; (ii) apical branching – the emergence of a new tip immediately behind a current tip; and (iii) lateral branching – the emergence of a new tip some distance behind a current tip. In *R. solani* new tips emerge from hyphal walls, such as in (ii) and (iii) above. However, the exact underlying mechanisms responsible for branching are unknown, although turgor pressure, possibly resulting from a build-up of tip-growth vesicles, and ionic gradients, have been implicated (see, for example, Prosser and Trinci, 1979; Gow and Gadd, 1995; Watters and Griffiths, 2001, and references therein). Consistent with the above hypotheses, we assume that the branching rate depends on the internal concentration of the growth limiting substrate. For simplicity (and in the absence of any experimental evidence to the contrary) we assume a linear relationship between the internal substrate concentration and the branching rate. Hyphal tips are lost through anastomosis with hyphal walls and similarly we assume a linear relationship between the anastomosis rate and the hyphal density. Therefore, we model f_p as

$$f_p = bs_i m - fmp, \tag{4}$$

where b denotes the branching rate per unit length of hypha per mole of internal substrate and f the per tip anastomosis rate per unit length of hypha.

Internal substrate is most generally absorbed autocatalytically, that is, substrate is used to acquire further substrate by active transport across the plasma membrane. The acquisition rate of the external substrate must therefore depend on the amount of internal substrate available to perform the active transport, the amount of external substrate available for absorption, and the hyphal surface area over which the absorption occurs. In previous models different approaches have been adopted. In Edelstein-Keshet et al., the uptake rate of substrate is viewed as being linearly proportional to hyphal density (representing the total area over which substrate is absorbed) and limiting with respect to the external substrate. However, no account is made of the uptake process being active. In Davidson (1998), account *is* taken of this energy requirement with the rate

being viewed as linearly proportional to s_i. However, the differing surface areas over which the absorption may occur is neglected. We combine these approaches by assuming the uptake rate depends (linearly) on both s_i and m. Moreover, in the experimental protocol under discussion here, the external substrate levels are such that limiting behaviour is unlikely to be observed. Indeed, most fungi are unlikely to encounter saturating conditions in natural growth habitats. Hence we model the uptake rate of substrate by $c_1 s_i m s_e$ where c_1 is a positive constant. The fungus expends energy (substrate) through uptake, translocation, growth and maintenance. The cost associated with substrate uptake is accounted for in the choice of the parameter c_1 (see below). Although passive translocation (i.e. diffusion) is a non-metabolic process, the active translocation of metabolites requires energy. We make the reasonable assumption that the cost of actively translocating material is proportional to the flux of that material ($|\boldsymbol{J}_i^{act}|$) with c_4 being the constant of proportionality. As previously explained, the extension of hyphal tips is the primary mechanism responsible for fungal growth (i.e. increase in biomass). Hence we assume the cost of growth is proportional to the flux of tips and is therefore modelled by $c_2|\boldsymbol{J}_p|$ where c_2 is a non-negative constant. Encapsulated also in this term are maintenance costs associated with such growth since, essentially, we assume that there is a maintenance cost associated with each tip. This is in line with the concept of a hyphal growth unit (Prosser and Trinci, 1979) and is a reasonable assumption where mycelial stasis does not occur. (This was the case in the experimental system over the observed time frame.) With these assumptions we model f_i as

$$f_i = c_1 s_i m s_e - c_2|\boldsymbol{J}_p| - c_4|\boldsymbol{J}_i^{act}|. \tag{5}$$

The final reaction term f_e corresponds to the rate of substrate depletion from the external environment. This term must have a similar form as the substrate uptake process derived above and therefore we set

$$f_e = -c_3 s_i m s_e, \tag{6}$$

where c_3 is a positive constant. To account for the imperfect conversion of external substrate to internal substrate (the cost of substrate uptake) we demand that $c_1 < c_3$.

Now we consider the flux terms, starting with $\boldsymbol{J}_p$, the term modelling tip movement. Migrating hyphal tips of many fungi (including *R. solani*) do not in general react to gradients of external nutrients (Gooday, 1975) although they may react to gradients of toxic metals (see, for example, Fomina et al., 2000). Indeed, hyphal tips in most mycelial fungi, including *R. solani*, grow predominantly in a straight line but exhibit small directional changes at seemingly random moments in time (see, for example, Dix and Webster, 1995). Essentially this directed growth is due to the structure of the hyphal walls and the way new wall material is incorporated at the tip. We therefore assume that two processes are involved in tip movement: a dominating deterministic (i.e. convective) component, accounting for the directed nature of tip movement, and a stochastic

(i.e. diffusive) element accounting for the small changes in the direction of hyphal growth. A consequence of the random element of tip movement is that the model captures the observed possibility of anastomosis in sparse mycelial networks: in the absence of this randomness, an individual model hyphal tip would not only avoid its own hyphae (grow in a straight line) but also avoid all other hyphae thus precluding anastomosis. We note however, that when the mycelial network is dense, a purely convective movement of tips would be sufficient to allow for the possibility of anastomosis.

It is clear that hyphal tip growth is possible only when energy (internal substrate) is supplied to the tip and, in particular, the tip velocity must be zero whenever the internal substrate concentration is zero. Consequently, we assume that both the convective and diffusive fluxes are zero whenever $s_i = 0$.

As commented previously, a single hypha may be regarded as the "trail" left behind a tip as it moves. Therefore, at the microscopic level, the directed nature of tip movement can be modelled by a convective flux acting such that a hyphal tip avoids its own biomass trail. At the continuum level, we therefore assume hyphal tip density convects in the direction of decreasing biomass density, capturing the commonly observed space-filling growth characteristic of many species of fungi. This general property is therefore modelled by the convection term$-v(s_i, \nabla m)p$. We assume the velocity vector $v(\cdot, \cdot)$ is a bilinear function (see also Prosser and Trinci, 1979, who likewise assumed a linear relationship between internal substrate concentration and tip velocity but neglected the directional nature of individual tip movements). The small variations in the growth direction of individual hyphal tips can be modelled at the continuum level by diffusion. We therefore include in tip movement the flux $-D_p(s_i)\nabla p$ where the diffusion coefficient $D_p(\cdot)$ is assumed to be a linear function. Therefore, combining the above observations, we model $\boldsymbol{J}_p$ as

$$\boldsymbol{J}_p = -vs_i p\nabla m - D_p s_i \nabla p, \tag{7}$$

where v and D_p are non-negative constants.

Now consider the flux $\boldsymbol{J}_i^{pas}$ corresponding to the diffusion of internal substrate inside the fungal mycelium. Recall that the internal substrate moves through a network of tubes. Therefore more material can diffuse through a dense network than through than a sparse network. Consequently the flux $\boldsymbol{J}_i^{pas}$ is assumed to depend on the density of active hyphae. For simplicity and in the absence of any experimental evidence to the contrary, we assume this is a linear relationship. Hence we model passive translocation as

$$\boldsymbol{J}_i^{pas} = -D_i m \nabla s_i, \tag{8}$$

where D_i is a species-dependent non-negative constant describing the diffusion of internal material.

Now consider the flux $\boldsymbol{J}_i^{act}$ corresponding to the active translocation of internal substrate through the fungal mycelium. In line with experimental evidence

(see, for example Olsson and Jennings, 1991), we assume that the fungus has the ability to move metabolites to mycelial regions exhibiting a demand for the resource. Since hyphal tips are primarily responsible for filamentous fungal growth (and are therefore likely to be the largest energy sinks), it is reasonable to assume that hyphal tips create this demand and thus we assume the active flux of internal substrate is directed up p-gradients. The substrate is translocated through a network of hyphae and, as in the formulation of $\boldsymbol{J}_i^{pas}$, the amount of material moved will depend on the density of hyphal network. Thus, making similar assumptions used in the derivation of $\boldsymbol{J}_i^{pas}$ in (8), we set

$$\boldsymbol{J}_i^{act} = D_a m s_i \nabla p, \tag{9}$$

where D_a is a non-negative constant describing the strength of the active translocation.

The external substrate is assumed to obey standard laws of diffusion and so we set

$$\boldsymbol{J}_e = -D_e \nabla s_e, \tag{10}$$

where D_e is a non-negative constant depending on the substrate and the growth medium.

Substituting (2)–(10) into (1) yields the model equations

$$\frac{\partial m}{\partial t} = |v s_i p \nabla m + D_p s_i \nabla p| - d_a m, \tag{11a}$$

$$\frac{\partial m'}{\partial t} = d_a m - d_i m', \tag{11b}$$

$$\frac{\partial p}{\partial t} = \nabla \cdot (v s_i p \nabla m + D_p s_i \nabla p) + b s_i m - f m p, \tag{11c}$$

$$\frac{\partial s_i}{\partial t} = \nabla \cdot (D_i m \nabla s_i - D_a m s_i \nabla p) + c_1 s_i m s_e - c_2 \left| v s_i p \nabla m + D_p s_i \nabla p \right| - c_4 \left| D_a m s_i \nabla p \right|, \tag{11d}$$

$$\frac{\partial s_e}{\partial t} = D_e \nabla^2 s_e - c_3 s_i m s_e. \tag{11e}$$

The model equations are to be solved in the square domain $(0, L)^2$ for some positive constant L with appropriate boundary conditions and initial data. Consistent with typical experimental protocol, we apply zero-flux boundary conditions since material (such as substrate) neither enters nor leaves the domain. The initial data is chosen to resemble a plug of mycelium placed onto a fresh

substrate medium and so we set

$$m(\boldsymbol{x},0) = \begin{cases} G_1(|\boldsymbol{x}-\hat{\boldsymbol{x}}|)m_0, & \text{if } |\boldsymbol{x}-\hat{\boldsymbol{x}}| \le \lambda, \\ 0, & \text{otherwise,} \end{cases} \tag{12a}$$

$$m'(\boldsymbol{x},0) = \begin{cases} G_1(|\boldsymbol{x}-\hat{\boldsymbol{x}}|)m_0', & \text{if } |\boldsymbol{x}-\hat{\boldsymbol{x}}| \le \lambda, \\ 0, & \text{otherwise,} \end{cases} \tag{12b}$$

$$p(\boldsymbol{x},0) = \begin{cases} G_2(|\boldsymbol{x}-\hat{\boldsymbol{x}}|)p_0, & \text{if } |\boldsymbol{x}-\hat{\boldsymbol{x}}| \le \lambda, \\ 0, & \text{otherwise,} \end{cases} \tag{12c}$$

$$s_i(\boldsymbol{x},0) = \begin{cases} G_3(|\boldsymbol{x}-\hat{\boldsymbol{x}}|)s_{i_0}, & \text{if } |\boldsymbol{x}-\hat{\boldsymbol{x}}| \le \lambda, \\ 0, & \text{otherwise,} \end{cases} \tag{12d}$$

$$s_e(\boldsymbol{x},0) = s_{e_0}(\boldsymbol{x}), \tag{12e}$$

for some distribution $s_{e_0}(\boldsymbol{x})$. The quantity λ represents the radius of the inoculum while $\hat{\boldsymbol{x}}$ denotes the centre of the inoculum and is taken to be at $(L/2, L/2)$, the midpoint of the square domain. The functions $G_i, i = 1, 2, 3$, have compact support and take a maximum value of unity. We henceforth set $G_i = 1$, $i = 1, 2, 3$.

The above model includes the following key advancements on previous modelling studies. For the first time, the directed nature of hyphal tip extension (the major cause of mycelial expansion) is modelled in a mechanistic way that allows for the possibility of straight-line growth in *any* spatial directions in response to environmental factors. (Previously, such directed growth had been modelled as being confined to predetermined directions). Furthermore, translocation is modelled as comprising active (metabolically-driven) *and* passive (diffusive) components that both allow for internal substrate movement in all spatial directions. In turn, this means that fungal growth on various experimental assays (see, for example, the agar tessellations described below) can be more accurately modelled and thus more quantitative predictions can be obtained.

The PDE system (11) is of mixed hyperbolic-parabolic type and describes the spatio-temporal evolution of densities. Any meaningful solution must therefore both "conserve mass" (that is, there is no "mass leakage" due to numerical approximation of the flux) and, importantly, preserve the positivity of all the variables. Many commonly used methods of numerical solution fail to simultaneously preserve both of these important properties (see examples in Roe, 1986; LeVeque, 1992; Boswell et al., 2003). Gerisch et al. (2001) considered a general system comprising a reaction-diffusion equation and a reaction-convection equation and developed a numerical method which preserved the positivity of the variables. The method was extended in Boswell et al. (2003) to treat a more complex system consisting of coupled reaction-diffusion-convection equations in one spatial dimension. In the following section we summarize an adaption of these methods which was employed to solve (11) while a more detailed description of the numerical scheme is given in Appendix A.

3. Model Calibration and Solution Method

3.1. Calibration and Rescaling

For direct comparison with experimental results, a specific calibration experiment was conducted to determine values for the model parameters and initial data. This calibration experiment concerned the growth of *R. solani* Kühn anastomosis group 4 (R3), (IMI 385768), in 2% glucose-mineral salts medium (w/v) (MSM) at 30°C. The medium was inoculated and after 15 h the mycelium was examined by visually inspecting enlarged images of several different regions. The approximate length of hyphae and number of hyphal tips per unit area were thus obtained. By counting the number of branches and anastomoses in a given region, the corresponding branching and anastomosis rates were estimated. Hyphal tip velocity was similarly estimated. Carbon concentrations in the growth medium were known and hence the uptake rates were calculated. See Boswell et al. (2002) for full details. The values obtained are replicated in Table 1, Appendix A.

As is detailed in Appendix A, the system variables and parameters have vastly different magnitudes. Large differences in the magnitudes of the system variables provide further complications in the accurate integration of the numerical scheme discussed below. To overcome this, the model variables (and consequently, model parameters) are rescaled (see Appendix A). However, the rescaled system is identical in structure to (11) and henceforth we simply refer to the latter unless specifically noted otherwise. In particular, all the figures below refer to the unscaled variables and thus represent predictions and hypotheses concerning the observed qualitative and quantitative properties of mycelial growth and function.

3.2. Summary of Numerical Solution Method

The model system is solved as follows. The domain $[0, L]^2$ is discretised into an $N \times N$ grid and the rescaled version of system (11) is discretised using a finite difference scheme based on the method of lines. Flux limiters are employed in the treatment of the convection terms to ensure the positivity of the solution while general flux schemes ensure mass conservation. During the spatial discretisation, the convective and diffusive fluxes are separated into x- and y-directed components and each component is treated independently in a similar fashion to that described in Boswell et al. (2003). The discretised system thus comprises an ODE system having stiff (reaction and diffusion) and non-stiff (convection) parts. A splitting method is used to integrate the ODE system where the stiff and non-stiff components are considered separately. The non-stiff terms are treated using an explicit, three-stage, second-order, Runge-Kutta method where the R-K matrix and weights are chosen to preserve positivity. The stiff components are treated using an implicit method based on the trapezoidal rule. The implicit method involves the solution of a linear system incorporating the Jacobian of the stiff terms in the ODE system. Since the stiff terms correspond to diffusion and reaction in both spatial directions, the Jacobian of the system will have a

bandwidth of $\mathcal{O}(N)$ irrespective of the ordering of the discretised variables in the construction of the Jacobian. A sparse solver is therefore used in the solution of the linear system. A variable time step method based on Richardson extrapolation is used to perform the integration and, consequently, linear interpolation is used to obtain numerical solutions at specific times. (See Appendix A for further details.)

4. Growth in Homogeneous Environments

4.1. Numerical results

The model equations (11) were solved using the method discussed above with initial data corresponding to a 4 mm diameter inoculum plug of *R. solani* placed in the centre of a 9 cm-diameter Petri dish uniformly filled with MSM. After an initial transient phase, the total hyphal density distribution $m + m'$ expanded from the initial data in a radially symmetric manner with constant radial velocity corresponding to approximately 0.5 cm day^{-1}. The total hyphal density was greatest at the point of inoculation and monotonically decreased towards the edge of the distribution ranging from 700 cm hyphae cm^{-2} at the centre to 0 at the edge. This quantitative and qualitative behaviour is entirely consistent with that observed in the calibration experiment and in line with many other similar experiments.

4.2. Approximation to biomass growth

After the rescaling the system parameters are still of different orders (see Table 1). This feature can be exploited by making suitable approximations and hence reducing (11) (or more properly its rescaled equivalent) to a more analytically tractable system.

The scaled parameters $\hat{b}$ and $\hat{f}$, the scaled branching and anastomosis rates respectively, are significantly larger than all other scaled parameters. Upon dividing the scaled version of (11c) by $\hat{f}$ and hereon dropping the hats for ease of exposition, we obtain

$$\frac{1}{f}\frac{\partial p}{\partial t} = \frac{1}{f}\nabla \cdot (v s_i p \nabla m + D_p s_i \nabla p) + \frac{b}{f} s_i m - mp. \tag{13}$$

From (13), if the gradients of m and p are not too large, the following approximate relationship can be derived:

$$s_i \approx \frac{f}{b} p. \tag{14}$$

On comparing this relation with solutions of the full system derived by numerical integration, it was found that (14) is indeed a good approximation in the centre of the biomass distribution where m and p are approximately spatially uniform.

(It holds for model growth in both homogeneous environments (see above) and heterogeneous environments (see the figures below).)

In the following analysis, we shall assume that (14) holds throughout the biomass distribution. If we also assume that the small terms associated with the cost of both biomass growth and the active translocation of internal substrate are negligible, then on substituting (14) into the scaled version of (11d) yields

$$\frac{\partial p}{\partial t} \approx \nabla \cdot \left(D_i m \left(1 - \frac{D_a}{D_i} p \right) \nabla p \right) + c_1 p m s_e. \tag{15}$$

As a further simplification, we assume that both biomass density and the external substrate concentration are constant. Furthermore, for fungal growth in uniform environments, the component of active translocation is significantly smaller than the diffusive component of translocation, i.e. $D_a \ll D_i$ (Boswell et al., 2002) and hence we assume $D_a/D_i = 0$. Thus, by introducing the constants $D \equiv D_i m$ and $\alpha \equiv c_1 m s_e$, equation (15) reduces to

$$\frac{\partial p}{\partial t} = D\nabla^2 p + \alpha p. \tag{16}$$

Here, the parameter D represents the "effective" diffusion coefficient of the internal substrate inside the biomass network and α represents the rate of tip creation in response to substrate uptake.

When augmented with initial data having compact support, as is the case in (12), the approximation (16) exhibits (asymptotically) a solution with whose leading edge is of wavefront form that travels with speed

$$c \approx 2\sqrt{\alpha D}, \tag{17}$$

(see, for example Britton, 1986; Murray, 1989). With the calibration given in Table 1, we obtain $c \sim 0.6$ cm day^{-1}. This compares well with the experimentally observed colony radial expansion rate of 0.5 cm day^{-1} (also predicted by the full model). We note, however, that (16), combined with positive initial data with compact support, will produce a solution that continues to increase in the centre of the distribution. Although an initial increase in tip density throughout the support of the biomass is observed experimentally and predicted by the full model, the tip density subsequently forms a distinct, large peak at the expanding outer edge of the biomass distribution with a uniform, quasi-steady value maintained in the interior. Hence, these properties are clearly a result of the more complex interactions detailed in the full model.

5. Heterogeneous Environments: Tessellated Agar Droplet System

5.1. Growth behaviour

A tessellated agar droplet system is described in Jacobs et al. (2002) where fungal growth was considered in a heterogeneous environment. Molten agar (MSM) was

pipetted onto the bases of 9 cm-diameter Petri dishes forming a hexagonal array comprising 19 circular droplets. Each agar droplet was 10 mm in diameter and the droplets were separated at their closest point of contact by a nutrient-free gap of 2 mm (see Fig. 1). In the current study, four combinations of tessellations are considered corresponding to using standard and glucose-supplemented MSM to form the interior and exterior droplets (see again Fig. 1). A 4 mm diameter inoculum of *R. solani* was placed onto the central droplet and the Petri dish was then sealed to prevent dehydration and contamination and inspected daily over a period of seven days.

Fig. 1 near here.

The numerical method outlined in Section 3.2 and Appendix A was applied to solve (11) using a spatio-temporal discretisation such that the numerical approximations were not significantly improved by further grid refinement. We set $L = 8$ (ensuring the domain was sufficiently large to contain the agar droplet tessellation), $\lambda = 0.2$ (the radius of the inoculum), while $s_{e_0}(\boldsymbol{x})$, the initial distribution of the external substrate, was defined appropriately for each tessellation. In the experimental system the diffusion of nutrients into the gaps between the agar droplets was not observed and therefore, as a first approximation to prevent such diffusion in the model system, we set $D_e = 0$.

In all four tessellations considered certain general properties were observed as follows. The model biomass covered the central droplet (see, e.g. Fig. 2) and expanded into the surrounding substrate-free space by translocating substrate from the central droplet region towards the "explorative" tips at the biomass edge. These tips subsequently bridged the narrow gap separating the droplets making a new substrate source available to the biomass. Through the uptake of this new resource, the sudden increase in internal substrate caused a profusion of branching (see equation (4)) and a marked increase in local tip density (see, e.g. Figs. 3 & 4). The active hyphal density increased in accordance with the higher tip density and resulted in greater hyphal densities on the droplet regions than in the substrate-free gaps (see, e.g. Fig. 2). (The highest tip and hyphal densities were recorded on supplemented MSM droplet regions with marginally greater hyphal densities on the droplet edges.). Subsequently material absorbed from these droplet regions (see, e.g. Fig. 4) was redistributed around the biomass network and used to support further growth in the substrate-free gaps (see, e.g. Fig. 2). All droplet regions were eventually covered.

Figs. 2,3,4,5 near here

As observed in Jacobs et al. (2002), greater biomass developed in regions representing low substrate droplets when high substrate droplets were also present in the tessellation (Fig. 5). For example, when the outer droplets represented unsupplemented MSM the final biomass density in this region was greater when

the inner droplets corresponded to glucose-supplemented MSM. The reverse case (i.e. when the central droplets were chosen to emulate unsupplemented MSM) yields similar observations upon varying the substrate used to make the outer droplets.

Further differences arose between the tessellations over the uptake rates of external substrate. The uptake rate in regions corresponding to the outer droplets was greatest when the inner droplets corresponded to glucose-supplemented MSM and least when the inner droplets corresponded to unsupplemented MSM. The active translocation of internal substrate further enhanced the ability of the biomass to uptake external substrate, a result in agreement with earlier modelling work (e.g. Boswell et al., 2002).

5.2. Acidification of the underlying media

Fungi produce various substances, for example acids, enabling the solubilisation of otherwise insoluble metal compounds (i.e. compounds that are insoluble in water) and that subsequently can be used to supplement colony growth (Gadd, 1999). This ability to solubilise metals is particularly influential in bioremediation and soil nutrient recycling. An accurate prediction of acidity levels may enhance the effective use of fungi in these roles.

Acidity is measured using the well-known pH scale

$$\mathrm{pH} = -\log_{10}[\mathrm{H}^+], \tag{18}$$

where H^+ denotes the concentration of free hydrogen ions. Jacobs et al. (2002) investigated acidity produced by *R. solani* in the tessellated agar droplet system described above. The agar was supplemented with a pH indicator (bromocresol purple) to give a visual guide to the acidification of the growth medium (Fig. 6 (a),(b),(c)). In particular, Jacobs et al. (2002) showed that acidification could only occur if glucose was present in the tessellated system, but, because of the translocation ability of *R. solani*, the carbon source need not be local to ensure acidification.

The acidification of the external substrate can be modelled by considering the processes responsible for proton (free hydrogen ion) production. We assume that protons originate from either the fungus or that they are already present in the growth medium. In addition, we reasonably assume that these protons undergo no further reactions and thus remain free in the environment during the modelled time interval. We denote the initial proton distribution in the external substrate by $B(\boldsymbol{x})$. Since a carbon source is necessary for the production of acidity by *R. solani*, it is therefore reasonable to relate the concentration of the internal substrate in the model system to the quantity of protons excreted by the fungus. To this end, we assume the creation of protons is linearly proportional to the internal substrate concentration. Thus the quantity of protons produced during the time interval $(0, t)$ is proportional to the integral of the internal substrate

concentration over that time interval. Therefore, consistent with the empirical definition of pH given in (18), we define the model pH as

$$\text{model pH at } (\boldsymbol{x}, t) = -\log_{10}\left(B(\boldsymbol{x}) + k\int_0^t s_i(\boldsymbol{x}, \xi)\mathrm{d}\xi\right), \tag{19}$$

where k is a non-negative constant. The integral in (19) can be approximated using a variety of methods but in all that follows we use the Trapezium rule with the discretised time steps introduced in the numerical discretisation (see Appendix A).

A simple experiment was conducted to calibrate (19) (see Jacobs et al., 2003, for a detailed description). A 9 cm diameter Petri dish was uniformly filled with glucose-supplemented MSM and the initial acidity of the medium was measured and recorded as pH 4.6. Therefore, the initial data for this calibration experiment gives $B(\boldsymbol{x}) \equiv 10^{-4.6}$. The medium was then inoculated with *R. solani* in the manner described above and the pH at 2 cm intervals along a diameter of the dish was measured and recorded after 4 days growth. The acidity was uniformly distributed across the dish with pH 3.9093 $\pm$0.02 (mean $\pm$ s.d.). The model equations (11) were solved in what represented a homogeneous environment and the model acidity expression defined in (19) was compared to that measured experimentally for a range of orders of k after a time corresponding to 4 days growth. The value of k giving the best fit between model and experimental acidity was determined to be $k = 10^{-5}$.

In the agar droplet experiments depicted in Fig. 6(a)–(c), the agar was buffered to have a neutral pH (i.e. pH 7) and consequently we set $B(\boldsymbol{x}) \equiv 10^{-7}$. The model equations (11) were solved using the above calibration and results compared to experimental observations (see Fig. 6). The pH indicator used in the experiment, bromocresol purple, has an operational range between pH 5.2 and pH 6.8 whereas the model expression (19) has no such limitation. For this reason, the model acidity is plotted with a colour scheme representing the limited pH range of bromocresol purple (Fig. 6 (d)–(f)) while a second colour scheme is applied showing the full acidification range (Fig. 6 (g)–(i)). The model acidification was determined at time intervals representing 24 h of biomass growth up to 72 h (Fig. 6 (d)–(i)). Initially, the model acidification was confined to regions representing the central droplet but as the biomass spread other droplets regions were covered and "acidified". The modelling predicts that the regions corresponding to the nutrient-free gaps separating the agar droplets are acidified to the same extent as the agar droplets themselves (Fig. 6 (g),(h),(i)). This could not be observed in the experimental system because of the gaps separating the droplets.

Fig. 6 near here.

6. Discussion

In this work we have developed a mathematical model that relates the properties of a fungal mycelium at the microscopic level to the growth and func-

tion observed at the macroscale. In particular, the movement of hyphal tips and translocation of internal substrate were carefully chosen to emulate known physiological properties. The model equations are of mixed hyperbolic-parabolic type and it is essential to the application that mass is conserved and positivity maintained. A numerical method was hence constructed that satisfied these demands. The model was calibrated for the fungus *Rhizoctonia solani* growing on glucose-mineral salts medium (MSM) and solved in both homogeneous and heterogeneous environments, the latter representing the agar droplet tessellations considered in Jacobs et al. (2002) (see also Fig. 1).

Model growth in uniform conditions reproduced the commonly observed radial expansion of biomass. Qualitative and quantitative features of the model solution compared well with those observed in the calibration experiment (and other similar experiments). An accurate approximation for the basic statistic, radial growth rate, was obtained from a simplified model which encapsulated colony growth at its simplest level. This perhaps suggests that colony expansion rate is dependent onlyon basic properties such as the average nutrient content of the environment and the connectedness of the network. Indeed, as suggested before (see Boswell et al., 2002), it may be that details such as tip distribution behind the leading front are more connected to exploitation of new resources than to explorative expansion of the mycelium. It would be interesting to test this easily verifiable method of calculating radial expansion for other species of fungi in a variety of habitats. However, this crude simplification is unable to capture the variety of observable phenomena produced by the full model and hence a study of the full system is essential with regards to the application.

For growth in tessellated droplet system, the model biomass density reflected the underlying substrate concentration; biomass was greatest on high substrate regions (corresponding to MSM augmented with glucose) and least on substrate-free regions. However, as in the experimental system, the translocation of internal substrate resulted in increased biomass on low substrate domains when high substrate patches were included in the tessellation: for example, the tessellation corresponding to the interior droplets formed using unsupplemented MSM and the exterior droplets formed using glucose-augmented MSM (see Figs. 2–4). In that tessellation, early biomass expansion occurred in a low substrate environment and consequently resulted in low biomass densities. When the outer droplets were encountered by the expanding biomass, a large resource pool became available and this was used to reinforce biomass on the inner droplets (Fig. 2). This biomass reinforcement occurred through either back-growth or *reverse translocation* (i.e. translocation in the opposite direction of growth). If the latter was responsible, then since active translocation moves substrate in the direction of increasing tip density and the tip density declines from the outer droplets towards the inner droplets (Fig. 3), it follows that reverse-translocation must have occurred through diffusion alone. This provides further evidence of the differing roles each component of translocation plays: diffusive translocation for explorative growth; active translocation for exploitation of resources. Although

biomass reinforcement was observed in Jacobs et al. (2002), no conclusions could be drawn on which process was responsible.

Irrespective of the tessellation, the final distribution of internal substrate behind the leading biomass edge was nearly uniform (e.g. Fig. 4). Indeed, once the entire tessellation had been covered by the model biomass, there was no indication of the original growth habitat from the internal substrate distribution. This common distribution arose despite the differences in biomass densities across the four tessellations (Fig. 5). A possible advantage of such an internal substrate distribution in a mycelium becomes clear when the environmental heterogeneity is viewed not only spatially, but also temporally. Recall from (6) that the uptake rate of external substrate in the model depends on the concentration of the internal substrate (as well as external substrate and active hyphal density). Hence, when the internal substrate is uniformly distributed there is an equal quantity of energy available for substrate uptake, irrespective of position behind the leading biomass edge. Therefore if internal metabolites are uniformly distributed in established fungal mycelial, this suggests that the mycelium is best equipped for the rapid exploitation of any newly encountered nutrient resource independent of where and when it arises.

The processes responsible for proton and acid production in fungi are complex (Gadd, 1999) although it is known that a carbon source is necessary to produce such metabolites (although, because of translocation, this carbon source need not be local, Jacobs et al., 2002). The production of acidity was easily observed in the experimental tessellated system by augmenting the growth medium with a pH indicator (bromocresol purple), with a colour change representing a change in acidity. In the current study, acidification is modelled by assuming that the production of protons is proportional to the concentration of internal substrate (which, recall, is considered to represent a carbon) and that the acidity at a point in space is proportional to the time integral of the internal substrate at that point. The model was calibrated via a specific growth experiment conducted in a homogeneous environment and then applied to the tessellated agar droplet system considered in Jacobs et al. (2002). The model made quantitative predictions extending those measurements made experimentally. In particular, the model generated data on the acidification in the gaps between the agar droplets and, importantly, gave data on pH values that lay outside the range of the pH indicator used in the experiment. Thus the model can be used to predict accurate levels of acidity in the growth medium in areas distant from nutrient (i.e. carbon) resources. Such predictions are clearly useful: the use of fungi as bioremediation/nutrient recycling agents may be improved by utilizing the deterministic link we propose between resource quantity and position and acidification of the surrounding environment. In particular, the use of fungi as bioremediation agents may be improved by making suitable amounts of carbon readily available to the fungus and exploiting its translocation abilities.

Certain fungi have significant uses as biological control agents against pests and diseases of plants (Whipps, 2001). Moreover, further experimental work is

ongoing to investigate their ability to transform toxic metals in the context of bioremediation (see, for example, Gadd, 1999). As nutrient recyclers, biocontrol agents and bioremediation agents, fungi are growing in environments exhibiting spatio-temporal heterogeneity. The modelling discussed above enhances the understanding of translocation processes and concomitant fungal function and may therefore assist in their biotechnological application.

Acknowledgments

GPB would like to thank Dr. A. Gerisch for useful discussions on the subjects of positivity and mass conservation and the authors thank the anonymous referees for helpful comments. This research was funded by the Biotechnology and Biological Sciences Research Council (BBSRC 94/MAF12243) as part of the Mathematics and Agriculture Food Systems Initiative. SCRI receives grant-in-aid from the Scottish Executive Environment and Rural Affairs Department.

References

Alexander, M. (1994). *Biodegradation and Bioremediation*. London: Academic Press.

Alexopolous, C. J., C. W. Mims, and M. Blackwell (1996). *Introductory Mycology* (4th ed.). New York: John Wiley and Sons.

Bailey, D. J., W. Otten, and C. A. Gilligan (2000). Saprophytic invasion by the soil-borne fungal plant pathogen *Rhizoctonia solani* and percolation thresholds. *New Phytologist 146*, 535–544.

Boddy, L. (1999). Saprotrophic cord-forming fungi: meeting the challenge of heterogeneous environments. *Mycologia 91*, 13–32.

Boswell, G. P., H. Jacobs, F. A. Davidson, G. M. Gadd, and K. Ritz (2002). Functional consequences of nutrient translocation in mycelial fungi. *Journal of Theoretical Biology 217*, 459–477.

Boswell, G. P., H. Jacobs, F. A. Davidson, G. M. Gadd, and K. Ritz (2003). A positive numerical scheme for a mixed-type partial differential equation model for fungal growth. *Applied Mathematics and Computation*. In press.

Britton, N. F. (1986). *Reaction Diffusion Equations and their Application to Biology*. New York: Academic Press.

Burgstaller, W. and F. Schinner (1993). Leaching of metals with fungi. *Journal of Biotechnology 27*, 91–116.

Cartwright, D. K. and H. W. Spurr (1998). Biological control of *Phytophthora parasitica var. nicotianae* on tobacco seedling with non-pathogenic binucleate *Rhizoctonia* fungi. *Soil Biology and Biochemistry 30*, 1879–1884.

Davidson, F. A. (1998). Modelling the qualitative response of fungal mycelia to heterogeneous environments. *Journal of Theoretical Biology 195*, 281–292.

Davidson, F. A. and S. Olsson (2000). Translocation induced outgrowth of fungi in nutrient-free environments. *Journal of Theoretical Biology 205*, 73–84.

Davidson, F. A., B. D. Sleeman, A. D. M. Rayner, J. W. Crawford, and K. Ritz (1996). Context-dependent macroscopic patterns in growing and interacting mycelial networks. *Proceedings of the Royal Society of London, Biological Sciences 263*, 873–880.

Dix, N. J. and J. Webster (1995). *Fungal Ecology*. London: Chapman and Hall.

Edelstein, L. (1982). The propagation of fungal colonies: a model for tissue growth. *Journal of Theoretical Biology 98*, 679–701.

Edelstein, L. and L. A. Segel (1983). Growth and metabolism in mycelial fungi. *Journal of Theoretical Biology 104*, 187–210.

Edelstein-Keshet, L. and B. Ermentrout (1989). Models for branching networks in two dimensions. *SIAM Journal on Applied Mathematics 49*, 1136–1157.

Fomina, M., K. Ritz, and G. M. Gadd (2000). Negative fungal chemotropism to toxic metals. *FEMS Microbiology Letters 193*, 207–211.

Gadd, G. M. (1992). Microbial control of heavy metal pollution. In J. C. Fry, G. M. Gadd, R. A. Herbert, C. W. Jones, and I. Watson-Craik (Eds.), *Microbial Control of Pollution*, pp. 59–88. Cambridge: Cambridge University Press.

Gadd, G. M. (1993). Interactions of fungi with toxic metals. *New Phytologist 124*, 25–60.

Gadd, G. M. (1999). Fungal production of citric and oxalic acid: importance in metal speciation, physiology and biogeochemical processes. *Advances in Microbial Physiology 41*, 47–92.

Gadd, G. M. (Ed.) (2001). *Fungi in Bioremediation*. Cambridge: Cambridge University Press. 481pp. ISBN: 0-521-78119-1.

Gadd, G. M. and J. Sayer (2000). Fungal transformations of metals and metalloids. In D. R. Lovley (Ed.), *Environmental Microbe-Metal Interactions*, pp. 237–256. Washington: American Society for Microbiology.

Gadd, G. M. and C. White (1993). Microbial treatment of metal pollution – a working biotechnology? *Trends in Biotechnology 11*, 353–359.

Garrill, A. (1995). Transport. In N. A. R. Gow and G. M. Gadd (Eds.), *The Growing Fungus*, pp. 163–181. London: Chapman & Hall.

Gerisch, A., D. F. Griffiths, R. Weiner, and M. J. Chaplain (2001). A positive splitting method for mixed hyperbolic-parabolic systems. *Numerical Methods for Partial Differential Equations 17*, 152–168.

Gerisch, A. and R. Weiner (2002). On the positivity of low order explicit Runge-Kutta schemes applied in splitting methods. *Computers and Mathematics with Applications In press*.

Gooday, G. W. (1975). Chemotaxis and chemotrophism in fungi and algae. In M. J. Carlile (Ed.), *Primitive Sensory and Communication Systems*, pp. 155–204. London: Academic Press.

Gooday, G. W. (1995). The dynamics of hyphal growth. *Mycological Research 99*, 385–394.

Gow, N. and G. M. Gadd (Eds.) (1995). *The Growing Fungus*. London: Chapman and Hall.

Heath, I. B. (1990). *Tip Growth in Plants and Fungi*. London: Academic Press.

Hundsdorfer, W., B. Koren, M. van Loon, and J. G. Verwer (1995). A positive finite-difference advection scheme. *Journal of Computational Physics 117*, 35–46.

Jacobs, H., G. P. Boswell, F. A. Harper, K. Ritz, F. A. Davidson, and G. M. Gadd (2003). Solubilization of metal phosphates by *Rhizoctonia solani*. *Mycological Research*. In Press.

Jacobs, H., G. P. Boswell, K. Ritz, F. A. Davidson, and G. M. Gadd (2002). Solubilization of calcium phosphate as a consequence of carbon translocation by *Rhizoctonia solani*. *FEMS Microbiology Ecology 40*, 65–71.

Jin, X., C. K. Hayes, and G. E. Harmon (1992). Principles in the development of biological control systems employing *Trichoderma* species against soil-borne plant pathogenic fungi. In G. F. Leatham (Ed.), *Frontiers in Industrial Mycology*, pp. 174–195. London: Chapman and Hall.

LeVeque, R. J. (1992). *Numerical Methods for Conservation Laws*. Lectures in Mathematics, ETH Zürich. Basel: Birkhäuser.

LeVeque, R. J. (1996). High-resolution conservative algorithms for advection in incompressible flow. *SIAM Journal on Numerical Analysis 33*, 627–665.

Littlefield, L. J., R. D. Wilcoxson, and T. W. Sudia (1964). Translocation of Phosphorus-32 in *Rhizoctonia solani*. *Phytopathology 55*, 536–542.

McCabe, P. M., M. P. Gallagher, and J. W. Deacon (1999). Microscopic observation of perfect hyphal fusion in *Rhizoctonia solani*. *Mycological Research 103*, 487–490.

Metting, F. B. (1992). Structure and physiological ecology of soil microbial communities. In F. B. Metting (Ed.), *Soil Microbial Ecology, Applications and Environmental Management*, pp. 3–25. New York: Marcel Dekker.

Morley, G. F., J. A. Sayer, S. C. Wilkinson, M. M. Gharieb, and G. M. Gadd (1996). Fungal sequestration, solubilization and transformation of toxic metals. In J. C. Frankland, N. Magan, and G. M. Gadd (Eds.), *Fungi and Environmental Change*, pp. 235–256. Cambridge: Cambridge University Press.

Murray, J. D. (1989). *Mathematical Biology* (2 ed.). London: Springer.

Ogoshi, A. (1987). Ecology and pathology of anastomosis and intraspecific groups of *Rhizoctonia solani* Kühn. *Annual Review of Phytopathology 25*, 125–143.

Olsson, S. (1994). Uptake of glucose and phosphorus by growing colonies of *Fusarium oxysporum* as qualified by image analysis. *Experimental Mycology 18*, 33–47.

Olsson, S. (1995). Mycelial density profiles of fungi on heterogeneous media and their interpretation in terms of nutrient reallocation patterns. *Mycological Research 99*, 143–183.

Olsson, S. and D. H. Jennings (1991). A glass fibre filter technique for studying nutrient uptake by fungi: the technique used on colonies grown on nutrient gradients of carbon and phosphorus. *Experimental Mycology 15*, 292–301.

Otten, W., C. A. Gilligan, C. W. Watts, A. R. Dexter, and D. Hall (1999). Continuity of air-filled pores and invasion thresholds for a soil-borne fungal plant pathogen, *Rhizoctonia solani*. *Soil Biology and Biochemistry 31*, 1803–1810.

Paustian, K. and J. Schnürer (1987). Fungal growth response to carbon and nitrogen limitation: a theoretical model. *Soil Biology and Biochemistry 19*, 613–620.

Persson, C., S. Olsson, and H.-B. Jansson (2000). Growth of *Arthrobotrys superba* from a birch wood food base into soil determined by radioactive tracing. *FEMS Microbiology Ecology 31*, 47–51.

Prosser, J. I. (1995). Mathematical modelling of fungal growth. In N. A. R. Gow and G. M. Gadd (Eds.), *The Growing Fungus*, pp. 319–335. London: Chapman and Hall.

Prosser, J. I. and A. P. J. Trinci (1979). A model for hyphal growth and branching. *Journal of General Microbiology 111*, 153–164.

Ritz, K. (1995). Growth responses of some soil fungi to spatially heterogeneous nutrients. *FEMS Microbiology Ecology 16*, 269–280.

Ritz, K. and J. W. Crawford (1990). Quantification of the fractal nature of colonies of *Trichoderma viride*. *Mycological Research 94*, 1138–1141.

Roe, P. L. (1986). Characteristic-based schemes for the Euler equations. *Annual Review of Fluid Mechanics 18*, 337–365.

Segel, L. A. (Ed.) (1980). *Mathematical models in molecular and cellular biology*. Cambridge, U.K.: Cambridge University Press.

Sietsma, J. H., H. A. B. Wosten, and J. G. H. Wessels (1995). Cell wall growth and protein secretion in fungi. *Canadian Journal of Botany 73 (Suppl. 1)*, S388–S395.

Sweby, P. K. (1984). High resolution schemes using flux limiters for hyperbolic conservation laws. *SIAM Journal on Numerical Analysis 21*, 995–1011.

Thornton, C. R. and C. A. Gilligan (1999). Quantification of the effect of the hyperparasite *Trichoderma harzianum* on the saprotrophic growth dynamics of *Rhizoctonia solani* in compost using a monoclonal antibody-based ELISA. *Mycological Research 103*, 443–448.

Tobin, J. M., C. White, and G. M. Gadd (1994). Metal accumulation by fungi – applications in environmental biotechnology. *Journal of Industrial Microbiology 13*, 126–130.

Trujillo, E. E. (1992). Bioherbicides. In G. F. Leatham (Ed.), *Frontiers in Industrial Mycology*, pp. 196–211. London: Chapman and Hall.

Wainwright, M. (1988). Metabolic diversity of fungi in relation to growth and mineral cycling in soil – a review. *Transactions of the British Mycological Society 90*, 159–170.

Watters, M. K. and A. J. F. Griffiths (2001). Tests of a cellular model for constant branch distribution in the filamentous fungus *Neurospora crassa*. *Applied and Environmental Microbiology 67*, 1788–1792.

Wessels, J. G. H. (1993). Wall growth, protein excretion and morphogenesis in fungi. *New Phytologist 123*, 397–413.

Whipps, J. M. (2001). Microbial interactions and biocontrol in the rhizosphere. *Journal of Experimental Botany 52*, 487–511.

Appendix A. Numerical Solution

A.1. Model Calibration and Rescaling

A calibration experiment providing estimates for the magnitude of system variables, parameter values and initial data for the model is outlined above and described in Boswell et al. (2002) (see also Table 1 below). Certain variables have vastly different magnitudes which complicates the procedure required to accurately and efficiently solve the system numerically. In particular, the adaptive time step integration procedure (see below) uses relative and absolute tolerances to compare approximations of the system advanced over a small time interval τ. In order to minimise the number of different tolerances required, the system variables are rescaled so that they are of the same order of magnitude and hence single relative and absolute tolerances may be applied for all variables (see also Boswell et al., 2003). The original model variables are hence recovered by a simple rescaling and so quantitative comparisons between model and experimental systems are possible.

We introduce the scaling factors m_s, p_s, s_s and define

$$\hat{m} = m m_s, \quad \hat{m'} = m' m_s, \quad \hat{p} = p p_s, \quad \hat{s_i} = s_i s_s, \quad \hat{s_e} = s_e s_s. \tag{A1}$$

We choose the rescaling factors such that the rescaled variables are $\mathcal{O}(0.1)$ and thus set $m_s = p_s = 10^{-3}$ and $s_s = 10^4$. The calibrated parameter values after rescaling are also shown in Table 1. If we subsequently rescale the system parameters as follows,

$$\hat{v} = \tfrac{v}{s_s p_s},\ \hat{D}_p = \tfrac{m_s D_p}{s_s p_s},\ \hat{d}_i = d_i,\ \hat{d}_a = d_a,\ \hat{b} = \tfrac{p_s b}{s_s m_s},\ \hat{f} = \tfrac{f}{m_s}, \hat{D}_i = \tfrac{D_i}{m_s},$$
$$\hat{D}_a = \tfrac{D_a}{m_s p_s},\ \hat{c_1} = \tfrac{c_1}{m_s s_s},\ \hat{c_2} = \tfrac{s_s c_2}{m_s},\ \hat{c_4} = c_4,\ \hat{D}_e = D_e,\ \hat{c_3} = \tfrac{c_3}{m_s s_s},$$

then it can be shown that the rescaled system is identical in structure to (11) (with system variables and parameters replaced by their rescaled equivalents).

Table 1 near here

A.2. Spatial Discretisation

The region $[0, L] \times [0, L]$ is discretised into an N-by-N grid with grid size $h = L/N$. We use the standard notation, e.g. $m_{kj}(t)$ to denote an approximation of $m(\boldsymbol{x}, t)$ where $\boldsymbol{x} = (kh, jh)$, $k, j = 0, 1, \ldots, N$.

The reaction terms in (11) are treated in the obvious manner and second-order central difference approximations are used in (11a) and (11d) for those reaction terms containing derivatives.

The flux terms in (11c), (11d) and (11e) can be separated into x- and y-directed fluxes and then further split into diffusive and convective fluxes. Thus, the fluxes are treated individually in a single spatial dimension (e.g. as in Boswell et al., 2003) and the numerical solution of the full system (11) can be constructed by summing the component parts.

The (non-linear) diffusive processes are treated using a mass-conserving second-order accurate scheme based on central differences (see again Boswell et al., 2003). However, the convection processes are harder to treat. We require a discretisation that preserves positivity and conserves mass. While the first-order upwind scheme satisfies these important properties, it can also introduce a large amount of numerical diffusion unless the spatial discretisation is sufficiently fine. On the other hand, high order spatial approximations often induce spurious oscillations into the solution (see, for example, LeVeque, 1992), which can result in negative values, especially when variables are small. Flux limiters provide a popular way of combining positivity and higher-order accuracy (e.g. Sweby, 1984; Roe, 1986; LeVeque, 1996).

As an example, consider the convection of hyphal tips in (11c). The convection in the x-direction at cell (k, j) is treated with the conservative scheme

$$x\text{-convection} = -\frac{1}{h}\left(F^p_{k+\frac{1}{2}\,j} - F^p_{k-\frac{1}{2}\,j}\right), \tag{A2}$$

for a suitable choice of general flux functions $F^p_{k+\frac{1}{2}\,j}$. We introduce w^p_{kj}, the x-directed velocity of the convective flux,

$$w^p_{kj} \equiv -vs_{i_{kj}}\frac{m_{k+1\,j} - m_{k-1\,j}}{2h}, \qquad k, j = 0, 1, \ldots, N,$$

and so the semidiscrete convective flux in the x-direction is then given by

$$f^p_{kj} = w^p_{kj} p_{kj}, \qquad k, j = 0, 1, \ldots, N.$$

Now introduce r^p_{kj} which encapsulates the ratio of x-directed fluxes around cell (k, j),

$$r^p_{kj} \equiv \frac{f^p_{k+1\,j} - f^p_{kj} + \epsilon}{f^p_{kj} - f^p_{k-1\,j} + \epsilon}, \qquad k, j = 0, 1, \ldots, N.$$

The parameter ϵ is a small number that ensures r^p_{kj} is well defined even when the surrounding fluxes are identical. In our applications we set $\epsilon = 10^{-30}$. The form of the general flux functions $F^p_{k+\frac{1}{2}\,j}$ will depend on the direction of flow. If the velocity is in the positive x-direction we set (see Hundsdorfer et al., 1995)

$$F^p_{k+\frac{1}{2}j} = f^p_{kj} + \frac{1}{2}\phi\left(r^p_{kj}\right)\left(f^p_{kj} - f^p_{k-1\,j}\right), \qquad k, j = 0, 1, \ldots, N, \tag{A3a}$$

where $\phi(r)$ denotes the *limiter function*. We use van Leer's limiter function

$$\phi(r) = \frac{r + |r|}{1 + r},$$

in order to obtain a second-order accurate discretisation. In Boswell et al. (2003) several limiter functions were compared against van Leer's limiter in a mixed-type system similar to that considered here. It was shown that consistent numerical solutions were obtained by using different limiter functions having the same

order of accuracy but van Leer's limiter function had better positivity properties (see also Gerisch et al., 2001). If the velocity is in the negative x-direction we reflect the indices around $k+\frac{1}{2}$ (see Gerisch et al., 2001, for details) and set

$$F^p_{k+\frac{1}{2}j} = f^p_{k+1j} + \frac{1}{2}\phi\left(\frac{1}{r^p_{k+1j}}\right)\left(f^p_{k+1\,j} - f^p_{xk+2\,j}\right), \tag{A3b}$$

We thus substitute either (A3a) or (A3b) into (A2) depending on the sign of w^p_{kj}. Similar schemes are used to treat the remaining convective fluxes in (11).

Zero flux boundary conditions are applied and are implemented as described in Boswell et al. (2003).

A.3. Time Integration

The spatial discretisation reduces the PDEs (11) to a system of $5(N+1)^2$ ODEs. It is the accurate and efficient time integration of this system of ODEs that benefits from the rescaling described above and it is the rescaled system of ODEs that is refered to below. (The spatial discretisation is not affected by such scaling.) The ODE system is a semidiscretisation of reaction, diffusion and convection terms and this property is exploited by suitably separating the system into two components. Specifically we use a (Strang) splitting method, as described in Boswell et al. (2003), separating the non-stiff (convection) and stiff (reaction and diffusion) components.

The non-stiff component is treated with a three-stage, second-order accurate Runge-Kutta method where the weights and measures are specifically chosen to preserve the positivity of the scheme (see Gerisch and Weiner, 2002, for details). The stiff components represent the reaction and diffusion processes and are treated with an implicit scheme based on the trapezoidal rule. This scheme involves the solution of $5(N+1)^2$ linear equations of $\mathcal{O}(N)$ bandwidth. In Gerisch et al. (2001), a method is described to reduce the computational costs in the integration of the stiff terms by splitting the reaction and diffusion terms into x- and y-directed components. This splitting technique replaces the solution of one linear system of bandwidth $\mathcal{O}(N)$ with the sequential solution of two linear systems of bandwidth $\mathcal{O}(1)$. However, such an approach is not possible with our model because certain reaction terms cannot be split into purely x- and y-directed terms. (Note that the use of the 1-norm in (11) would generate a system which can be additively split but that the crucial property of path length, i.e. the absolute value of the fluxes, would be over-estimated resulting in inaccurate approximations of the PDE system.) In our application, the linear system is written in sparse form to reduce storage space and the NAG routines `F01BRF` and `F04AXF` are used to obtain a solution. The first routine performs an LU factorisation of the sparse matrix (with optional pivoting) while the second routine solves the factorised system.

To further reduce computational costs, the ODE system is solved using a variable time step method. The time step selection strategy is based on Richardson

extrapolation considering accuracy alone and does not account for the positivity of the solution, i.e. the time step is allowed to exceed the sufficient condition for positivity which may be determined from the integration method above. (Note that this does not affect the positivity of the spatial discretisation.) However, this approach has not lead to negative solutions in any of our examples which may be because of the good positivity properties elsewhere in the discretisation (see Gerisch and Weiner, 2002).

The method is implemented by advancing the numerical solution over a time τ and comparing the approximations when time steps of size τ and $\tau/2$ are used. If a global error (comprising local relative and absolute errors) is below some user-defined tolerance parameter *tol*, the approximation obtained with time step $\tau/2$ is accepted, otherwise a new approximation is sought with a smaller value of τ. See Boswell et al. (2003) for details.

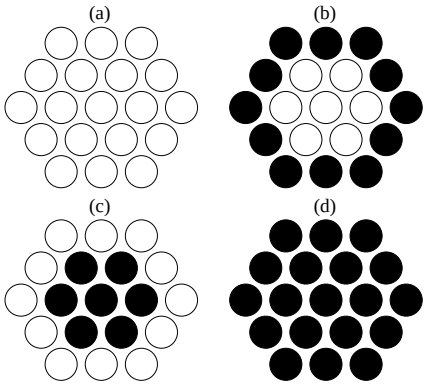

Figure 1: The hexagonal array used in Jacobs et al. (2002) consists of 19 agar droplets of 10 mm diameter positioned 2 mm apart. We consider the four distinct tessellations (out of a total of 16) shown in (a) to (d). The black and white circles respectively denote droplets made from glucose-supplemented and unsupplemented agar.

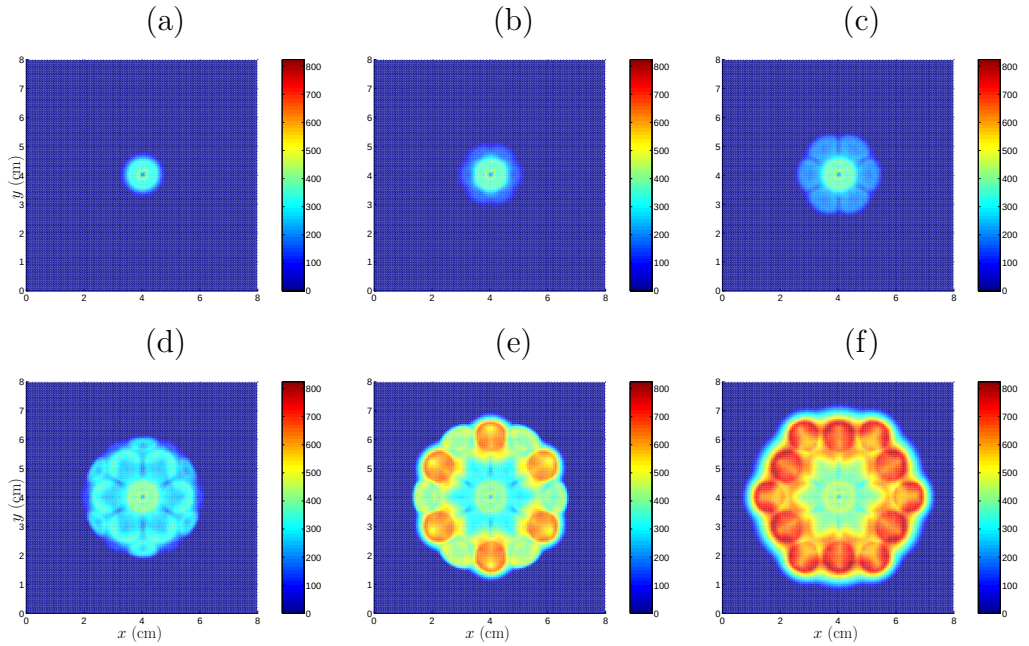

Figure 2: The total hyphal density $(m + m')$ is shown in units of cm hyphae cm^{-2} at times corresponding to (a) $t = 1$ day, (b) $t = 2$ days, (c) $t = 3$ days, (d) $t = 4$ days, (e) $t = 5$ days and (f) $t = 6$ days. Notice that once the biomass reaches the outer droplets, growth is reinforced on the inner droplets (via translocation). The model equations were solved with initial data representing the tessellation shown in Fig. 1(b). The model parameter values are given in the text while the parameter values used in the numerical solution are $N = 200, tol = 10^{-5}$ (see Appendix A).

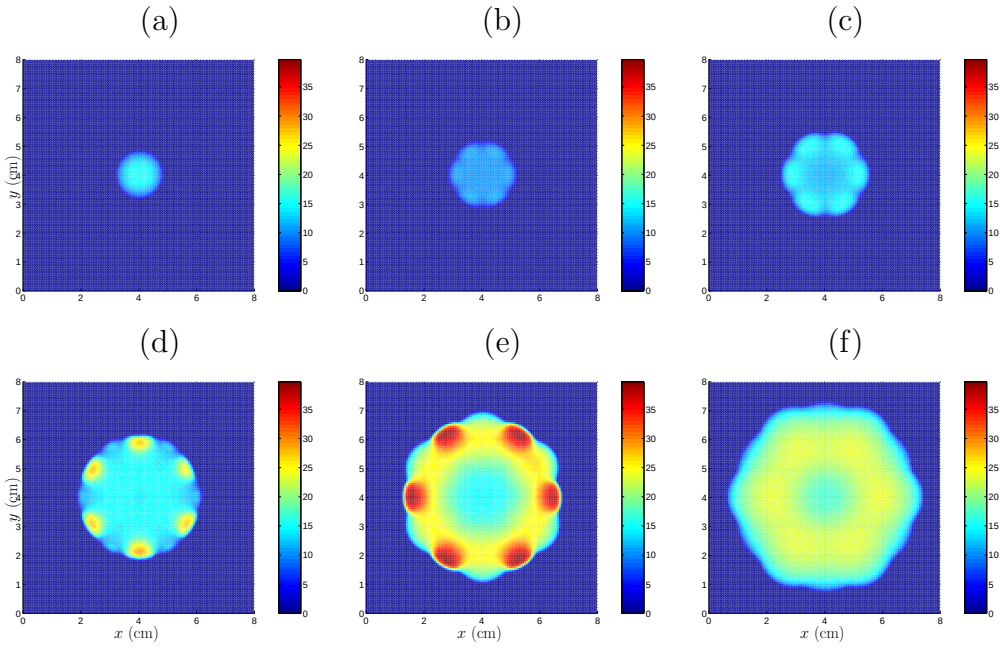

Figure 3: The tip density (hyphal tips cm^{-2}) is shown at times representing (a) $t = 1$ day, (b) $t = 2$ days, (c) $t = 3$ days, (d) $t = 4$ days, (e) $t = 5$ days and (f) $t = 6$ days. Notice that there is a profusion of branching in regions corresponding to the glucose-supplemented medium. The model equations were solved with initial data representing the tessellation shown in Fig. 1(b). The model parameter values are given in the text while the parameter values used in the numerical solution are $N = 200$ and $tol = 10^{-5}$ (see Appendix A).

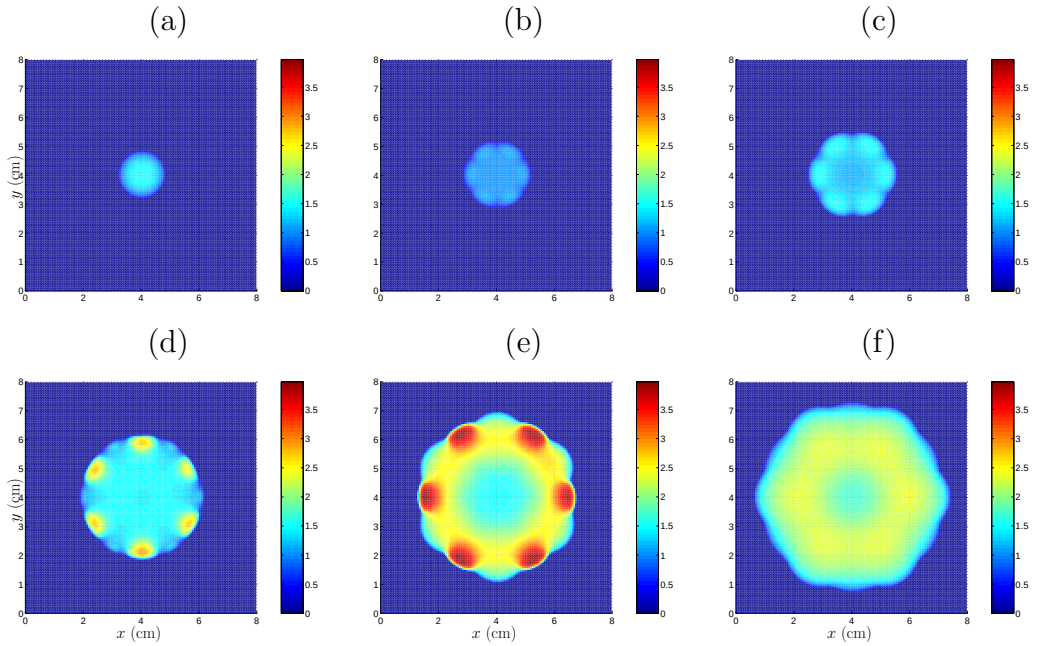

Figure 4: The internal substrate concentration (mol cm^{-2}) is shown at times representing (a) $t = 1$ day, (b) $t = 2$ days, (c) $t = 3$ days, (d) $t = 4$ days, (e) $t = 5$ days and (f) $t = 6$ days. Notice that the substrate is rapidly acquired from the agar droplets and that it is translocated throughout the model biomass resulting in a near-uniform distribution. The model equations were solved with initial data representing the tessellation in Fig. 1(b). The model parameter values are given in the text while the parameter values used in the numerical solution are $N = 200$ and $tol = 10^{-5}$ (see Appendix A).

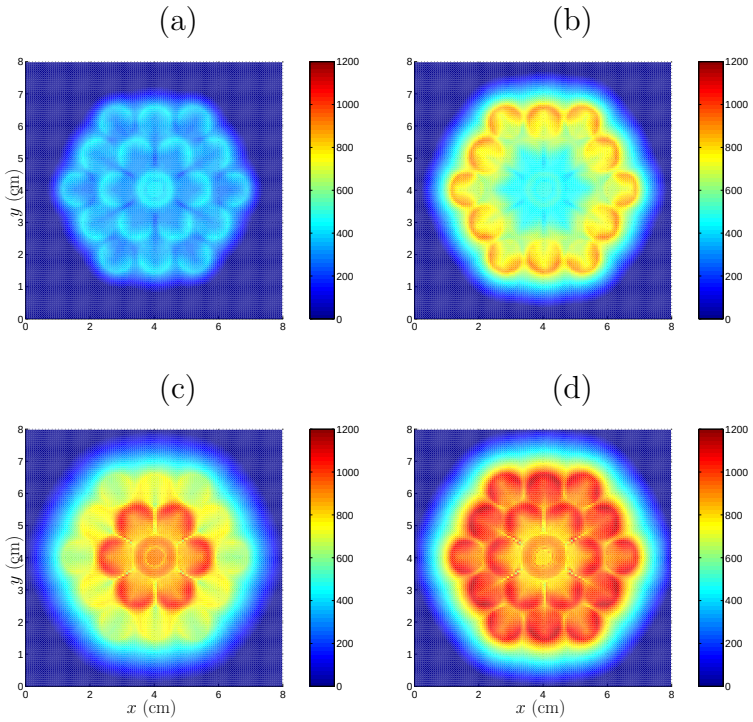

Figure 5: The total hyphal density (cm hyphae cm^{-2}) at a time representing 7 days is shown across four different tessellations. The tessellations (a)–(d) respectively correspond to those in Fig. 1 (a)–(d). Notice the the final hyphal density is greatest on high substrate regions and that the hyphal density on low substrate regions is increased by the presence of high substrate levels elsewhere. The model parameter values are given in the text while the parameter values used in the numerical solution are $N = 200$ and $tol = 10^{-5}$ (see Appendix A)

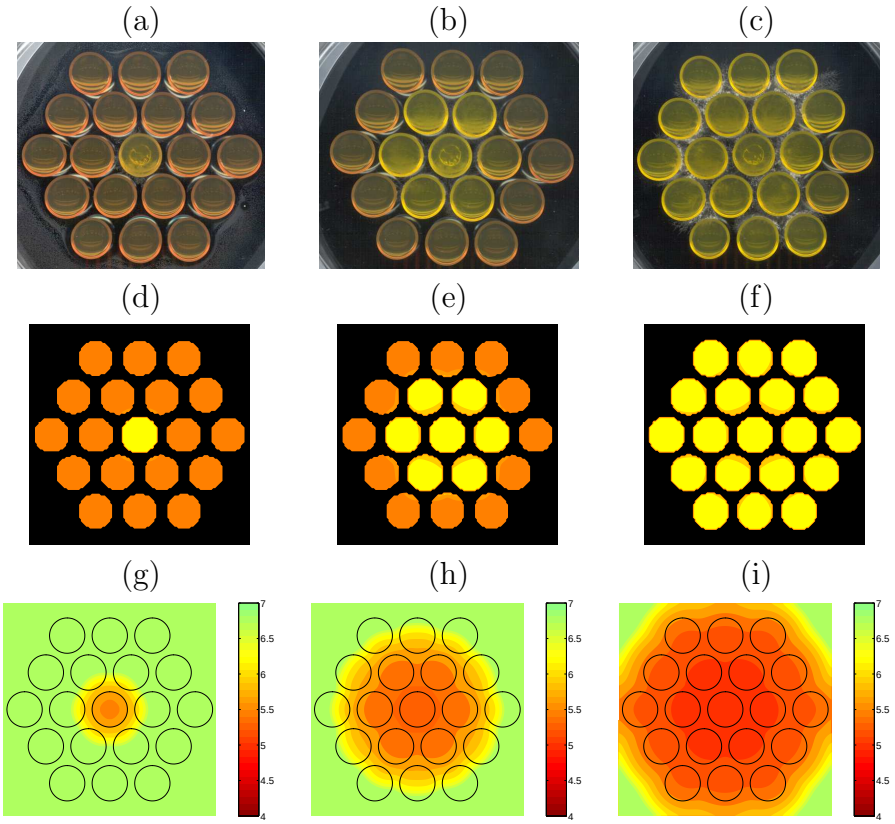

Figure 6: The experimental acidification is shown after (a) 1 day, (b) 2 days and (c) 3 days while the model equivalent is shown in (d), (e) and (f) respectively. The pH indicator bromocresol purple can only distinguish acidity between pH 5.2 and pH 6.8 and therefore, in accordance with this fact, we set the colour scale in (d)–(f) appropriately. Notice that (d), (e) and (f) do not depict acidity in the regions representing the gaps between the agar droplets and do not demonstrate acidification in excess of pH 5.2. To this end, (g), (h) and (i), respectively corresponding to 1,2 and 3 days growth, show the model acidification determined by (19) with no such restrictions on the colour scheme and where the colour scheme represents a (standard) universal pH indicator. The circles in (g)–(i) denote the location of the agar droplets. The model equations are solved with initial data representing the tessellation in Fig. 1(d) using the calibration shown in Table 1. The model acidification is obtained as described in the text. The model parameter values are given in the text while the parameter values used in the numerical solution are $N = 200$ and $tol = 10^{-5}$ (see Appendix A)

Parameter/Initial data	*Value*	*Rescaled value*
m_0	100 cm^{-1}	0.1
m_0'	0 cm^{-1}	0
p_0	100 hyphal tip cm^{-2}	0.1
s_{i_0}	4×10^{-5} mol glucose cm^{-2}	0.4
s_{e_0}	3×10^{-5} mol glucose cm^{-2}	0.3
v	5 cm^5 day^{-1} mol^{-1}	0.5
d_a	5×10^{-1} day^{-1}	0.5
d_i	0 day^{-1}	0
b	10^7 branches cm^{-1} hyphae day^{-1}	10^3
f	10^1 fusions in cm of hyphae day^{-1}	10^4
c_1	9×10^2 cm $(\text{mol glucose})^{-1}$ day^{-1}	90
c_2	10^{-7} mol glucose cm^{-1} per tip	1
c_3	10^3 cm $(\text{mol glucose})^{-1}$ day^{-1}	10^2
c_4	10^{-8} cm^{-1}	10^{-8}
D_p	10^{-5} cm^4 day^{-1} mol^{-1}	0.1
D_i	10^{-2} cm^3 day^{-1}	10
D_a	10^{-5} cm^3 day^{-1} per tip	10
D_e	0.3456 cm^2 day^{-1}	0.3456
λ	0.2 cm	0.2

Table 1: The paameter values and initial data used in the model are obtained from a calibration experiment (see Boswell et al., 2003, for details). The original parameter values are given along with rescaled values (see text for explanation).